Ultrasonic Ranging Sensor using Simultaneous Emissions from Different Transducers

Álvaro Hernández, Jesús Ureña, Juan J. García, Manuel Mazo, *Member, IEEE*, Daniel Hernanz, Jean-Pierre Dérutin, and Jocelyn Sérot

***Abstract*—In recent applications based on ultrasound, several ultrasonic transducers have been geometrically and electronically associated to constitute a global sensor. There are several different methods used to process the ultrasonic signals obtained from these transducers. In this work, multimode techniques using Golay complementary sequences are proposed for processing the ultrasonic signal. The system increases scan rate, precision, and reliability. It is also capable of echo discrimination, allowing simultaneous measurements to be made and detection of the same obstacle by different transducers without cross-talk problems. The real-time implementation of the algorithm is presented on a field-programmable gate array (FPGA) device.**

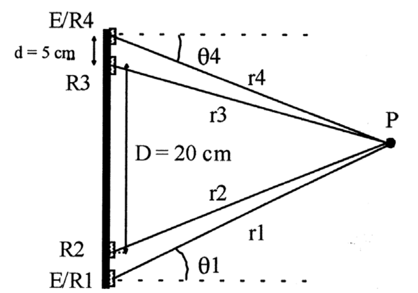

Fig. 1. Sonar sensor composed of four ultrasonic transducers.

I. Introduction

Classical processing techniques used in ultrasonic transducers for mobile robots are based in time-of-flight (TOF) measurement. One isolated transducer is excited by a squared signal and then the system waits for possible echoes. Detection is normally performed by integrating and threshold-crossing the received signal. The problems with this mode of operation are well-known and referenced in previous works [1]–[4]:

- Measurements must be carried out independently for each transducer. The transducers cannot be excited simultaneously to avoid cross-talk problems. It takes a long time to perform an environmental scan, as it must be sequential.
- Furthermore, after a pulse is emitted, the signal is received by only one transducer (usually the same one that emitted the pulse), which means the probability of certain obstacles not being detected due to specular reflections is relatively high.
- Measured distance precision is reduced. It may be enough for some applications, but not for processing measurements from different transducers in more sophisticated systems. In these systems it is possible to determine reception angles, or perform reflector classification (i.e., walls, edges, corners) and mapping, if TOF have enough precision and reliability.

In this work, a new low-level processing technique for ultrasonic signals, which overcomes most of the problems mentioned in the previous paragraphs, and its implementation on a configurable device are presented. The following section introduces the proposed sonar system, which is suitable for use in mobile robots. Section III contains an explanation of the low-level algorithm, analyzing its requirements and constraints. Hardware implementation is illustrated in Section IV. Section V describes the results obtained, and, finally, some conclusions are discussed in Section VI.

II. Ultrasonic Sensor Module

The sensor configuration used can be seen in Fig. 1. It is the geometrical association of four transducers. Every two transducers constitutes a "vector sensor," able to measure distances and reception angles [5]. These transducers are very close to each other to minimize correspondence problems and to confirm the reception of echoes from the same reflector by both transducers [5], [6]. In Fig. 1, P is a possible reflector detected by the four transducers (r_1, r_2, r_3, and r_4).

This sensor configuration type and its use have been described in [6], [7] in order to classify different reflector types. If it is desirable to improve the capability of these sensors, it is important to achieve the following features:

- Simultaneous reception of the reflected signal by all the transducers ($E/R1$, $R2$, $R3$ and $E/R4$). In this way, four TOF measurements can be combined in high-level algorithms from just one emission. Furthermore, the probability of obstacle detection is increased

Manuscript received February 12, 2003; accepted July 2, 2004. This work was supported by the Spanish Ministry of Science and Technology under Grants COO1999-AX049 and HF2000-0017.

Á. Hernández, J. Ureña, J. J. García, M. Mazo, and D. Hernanz are with the Electronics Department, University of Alcalá, Alcalá de Henares, 28806 Madrid, Spain (e-mail: alvaro@depeca.uah.es).

J. P. Dérutin and J. Sérot are with LASMEA Laboratory (U.M.R. 6602 C.N.R.S.), Blaise Pascal University, 63177 Aubière Cedex, France.

0885–3010/$20.00 © 2004 IEEE

and problems related to specular reflections are reduced.

- Echo discrimination can distinguish which emitter transmitted the signal ($E/R1$ and $E/R4$ in Fig. 1), even if the emissions from both transducers are simultaneous. This is possible thanks to the ultrasonic pulse codification used in each emitter. It is important to perform simultaneous measurements, in order to be able to:
  - Reduce scanning time and thus detect obstacles or objects more quickly.
  - Obtain simultaneous reception of echoes for the same reflector by all the transducers, from two different emission sources.

For some high-level tasks (such as reflector classification), it has been shown [6] that it is necessary to achieve echo reception for the same reflector from different emission sources. In classical systems, this can be carried out only in a sequential way; so first one transducer emits, and all of the transducers detect possible echoes. Then the process is repeated for the other emitter. This method implies that the vehicle and any obstacles must be stationary in order to fix similar geometrical conditions for both measurements. The system proposed here allows simultaneous emissions with echo discrimination, so measurements can be carried out with moving robots or vehicles, as well as moving obstacles.

III. Time-of-Flight Determination Using Golay Sequences

The possibility of utilizing Golay complementary sequence pairs to determine TOFs has been demonstrated in previous works [8], [9]. These pairs are composed of two sequences, with the addition of independent autocorrelation functions, which provide an output signal as that shown in (1):

$$C_{AA}[n] + C_{BB}[n] = \begin{cases} 2N, & n = 0 \\ 0, & n \neq 0 \end{cases}, \tag{1}$$

where $A[n]$ and $B[n]$ are the pair of Golay complementary sequences with values in the set $\{-1, +1\}$; N is the number of bits or their length; and C_{xy} is the correlation between signal x and signal y (i.e., C_{AA} and C_{BB} are autocorrelation functions).

To allow simultaneous emissions from two transducers, it is necessary to obtain two orthogonal Golay sequence pairs [8], i.e., $[A_1, B_1]$ and $[A_2, B_2]$. These pairs are orthogonal if they meet (2):

$$C_{A_1A_2}[n] + C_{B_1B_2}[n] = 0 \ \ \forall n. \tag{2}$$

Fig. 2 shows a 32-bit complementary sequence pair, A and B, and the result of adding the autocorrelation functions. A peak can be observed, with an amplitude of $2 \cdot N$. On the other hand, Fig. 3 shows two 32-bit orthogonal Golay pairs, $[A_1\, B_1]$ and $[A_2\, B_2]$, where it can be observed that their cross-correlation function is null.

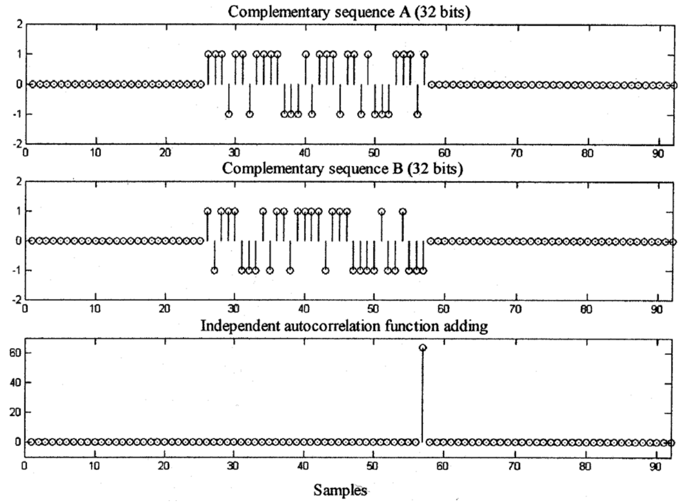

Fig. 2. Example of a 32-bit Golay complementary sequence pair $[A\,B]$.

For the emission sequence, a type of digital classical QPSK modulation has been implemented, in which components I and Q have been associated with each pair's sequences. In [9] a different method is proposed, based on the consecutive emission of complementary sequences A_i and B_i. However, this solution has been discarded, as it requires a static environment, with nonmoving sensors or reflectors. In this way, QPSK modulation allows both complementary sequences to be emitted simultaneously, so motion can be supported by the final system. Eq. (3) reflects mathematically how to compute the signal $e_i[n]$ emitted by transducer i.

$$\begin{aligned} e_i[n] &= A_i[n] * S_I[n] + B_i[n] * S_Q[n] \\ &= \sum_{k=0}^{N\cdot M\cdot m-1} A_i\left[\frac{k}{M\cdot m}\right]\cdot S[n-k] \\ &\quad + \sum_{k=0}^{N\cdot M\cdot m-1} B_i\left[\frac{k}{M\cdot m}\right]\cdot S\left[\left(n-\frac{M}{4}\right)-k\right], \end{aligned} \tag{3}$$

where M is the number of samples per symbol $S[n]$ period (related to the sampling frequency f_S used in the receiver's acquisition system); m is the number of periods per symbol; and N is the number of bits of Golay sequence length. We assume that $f_S = 400$ kHz, $M = 8$, $m = 2$, and $N = 32$, but it is possible to modify these values. The signals $A_i[n]$ and $B_i[n]$ constitute the Golay complementary pair assigned to emitter i. The first is associated to component I (in-phase), and the second, sequence $B_i[n]$, is related to component Q (quadrature). On the other hand, the signals $S_I[n]$ and $S_Q[n]$ are the carrier signals for components I and Q, respectively, and are obtained from the same symbol $S[n]$ with its corresponding phase. The symbol is chosen to focus the emission at the maximum frequency response of the ultrasonic transducer (50 kHz).

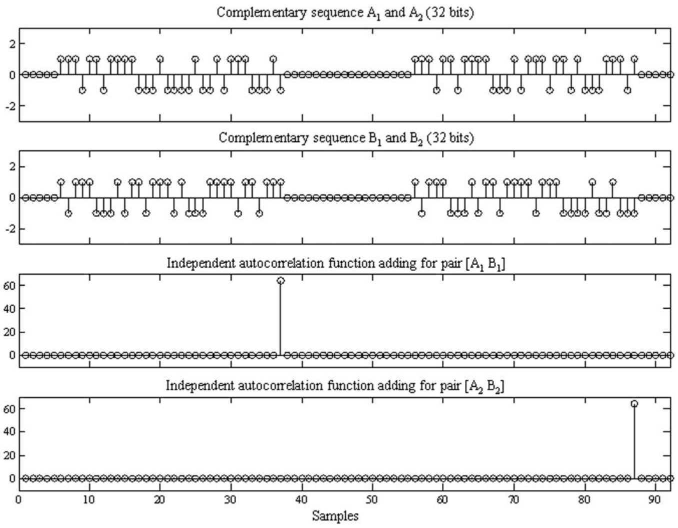

Fig. 3. Example of two orthogonal Golay pairs, $[A_1\, B_1]$ and $[A_2\, B_2]$, with a null cross-correlation.

In the reception stage, the demodulator performs a correlation between the signal $r_i[n]$ received by transducer i and the symbol $S[n]$ used in emission. This allows components $I_i[n]$ and $Q_i[n]$ to be obtained as shown in (4):

$$I_i[n] = C_{rS_1}[n] = \sum_{k=0}^{M\cdot m-1} r_i[k+n]\cdot S[k],$$
$$Q_i[n] = C_{rS_Q}[n] = \sum_{k=0}^{M\cdot m-1} r_i[k+n]\cdot S\left[k-\frac{M}{4}\right]. \quad (4)$$

Once the two modulation components have been obtained, the search for the Golay sequences is carried out using a second correlation, each one in its corresponding component, I or Q. This second correlation for the search of the sequence $A_i[n]$ in component I is described mathematically in (5). The expression is similar for the detection of sequence $B_i[n]$ in component Q.

$$S_{IA_i}[n] = C_{IA}[n] = I_i[n\cdot(m\cdot M)]\cdot A_i[n] = \sum_{k=0}^{N-1} I_i[k\cdot(m\cdot M)+n]\cdot A_i[k]. \quad (5)$$

Finally, results from both correlations are summed together and a peak detector is used to determine the precise moment the echo arrives.

As described previously, processing is generalized in each receptor for the detection of two different and orthogonal Golay sequence pairs (Fig. 4), in which the block diagram for the emitter/receiver 1 ($E/R1$) can be seen. Its emission is coded by the pair $[A_1,\, B_1]$, and it discriminates echoes from itself or from the other emitter. The block diagram includes a general sequencer module that operates the different tasks in the algorithm, managing the use of common resources, and synchronizing the communication of the intermediate results.

If the block diagram for only one receiver (not emitter) is considered, modules related to the emitting process are not needed (QPSK modulation and emission modules in Fig. 4).

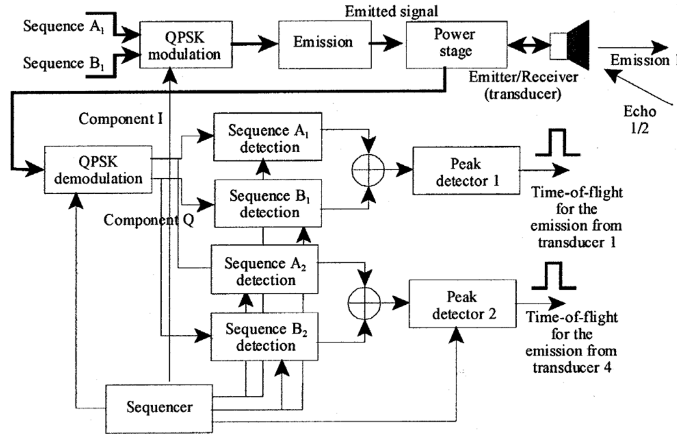

Fig. 4. Simplified scheme of the processing system in the $E/R1$ transducer.

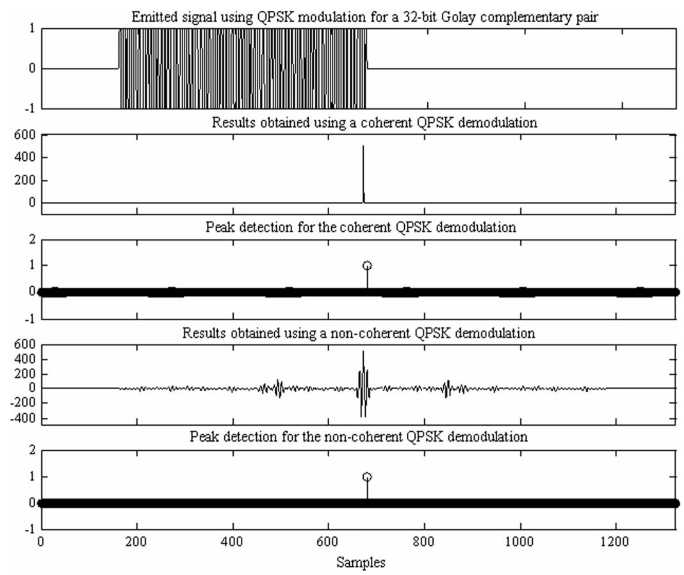

Fig. 5. Simulated example of the proposed algorithms for a sequence length of 32 bits.

Fig. 5 contains a simulated example which includes the QPSK demodulation processing. As can be observed, the coherent demodulation provides ideal results with no sidelobes. Nevertheless, it is not possible to synchronize modulation in a sonar system, as distances to reflectors are not known *a priori.*

Due to the use of a noncoherent demodulation, some sidelobes appear close to the main one. This implies a reduction in the signal-to-noise ratio (SNR) supported by the system, which must be taken into account. However, a constant distance, depending on the length of the modulation symbol, separates the two main sidelobes, so they can easily be discarded by a suitable configuration of the peak detector module.

The use of a noncoherent demodulation implies the degradation of the cross-correlation between orthogonal

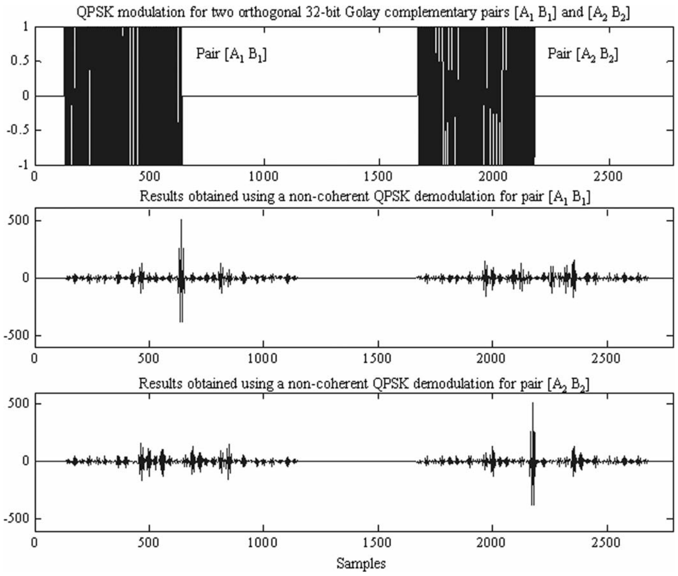

Fig. 6. Detection of two orthogonal 32-bit Golay complementary pairs using a noncoherent QPSK demodulation.

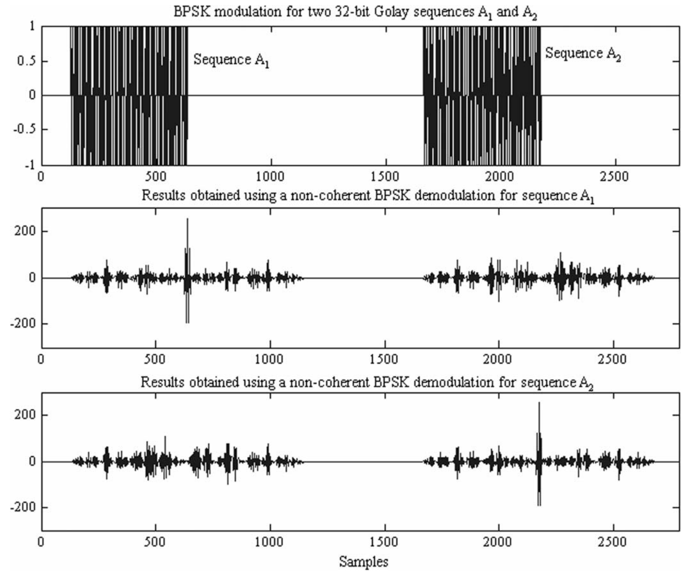

Fig. 8. Detection of two 32-bit Golay sequences using a noncoherent BPSK demodulation.

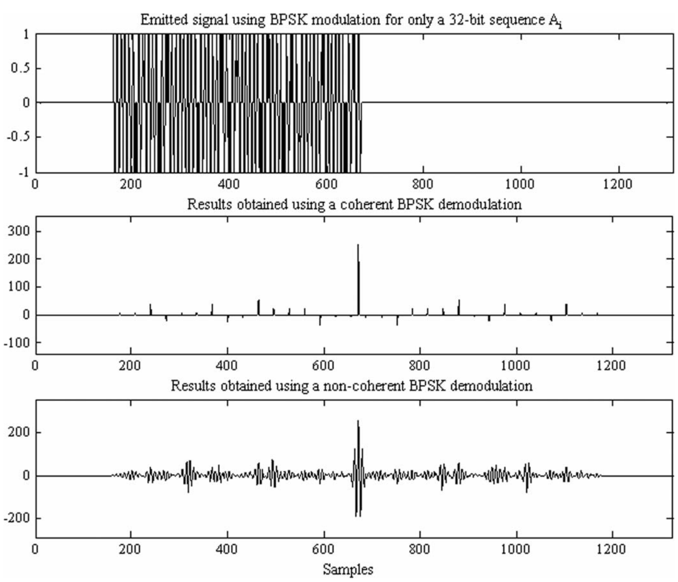

Fig. 7. Evaluation of the algorithm using only one Golay complementary sequence A_i.

Golay pairs, which is not null anymore. Nevertheless, values from the cross-correlation are enough lower, so the primary lobes originating from the echoes can be clearly identified (Fig. 6).

As can be seen in Fig. 7, if only one Golay complementary sequence is used, the resulting peak is only equal to N, as opposed to $2 \cdot N$. Furthermore, it is not even possible to obtain a total sidelobe cancellation for coherent demodulation conditions. The use of a Golay complementary pair $[A_i\, B_i]$ indicates a total sidelobe cancellation can be achieved, as has been shown before (see Fig. 5).

On the other hand, using only one complementary sequence implies a loss in the orthogonal properties, as can be observed in Fig. 8. Now, the main lobes are not so high, compared to the sidelobes from the cross-correlation, so the system performance is worse.

It is possible to analyze the value of main lobes and sidelobes, depending on the various possibilities: coherent/noncoherent demodulation, Golay pair/sequence, and sidelobes from the autocorrelation/cross-correlation function. Table I shows some interesting figures about the relationship between main lobes and sidelobes. It is important to remark that the two sidelobes closer to the main lobe have not been considered in Table I, since they can be eliminated using a window-based peak detector (see Section IV). For the noncoherent detection, the use of a Golay pair with a QPSK modulation implies improvements in cross-correlation sidelobes to main lobes ratios, compared to the use of only one sequence -0.44 for a pair, instead of 0.30 for only one sequence. In this way, the use of the whole Golay complementary pair, and its emission by means of QPSK modulation, is the most suitable solution for the proposed system.

A. Efficient Golay Correlator Algorithm

An optimized method for obtaining Golay sequence pairs with a length of $N = 2^s$ is explained in [10], where s is the number of bits of the sequence seed $(w_1, w_2, \ldots w_s)$. It is possible to generate a Golay sequence pair and also to design an efficient Golay correlator (EGC) using this particular seed. This correlator simplifies the detection process of Golay complementary sequences A and B. Fig. 9 shows the EGC block diagram.

In Fig. 9, D_s signifies a delay $D_s = 2^{Ps}$; Ps is any permutation of numbers $\{0, 1, \ldots, s-1\}$, represented as $\{w_1, w_2, \ldots w_s\}$; and $C_{rA}[n]$ and $C_{rB}[n]$ are the correlation results between the input signal $r[n]$ and the searched sequences A and B.

TABLE I
Comparison Between Main Lobes and Sidelobes from Autocorrelation and Cross-Correlation, Considering the Type of Demodulation (Assuming Input Signal Between −1 and +1).

		Main lobe	Sidelobes from autocorrelation	Sidelobes from cross-correlation
Golay pair	Coherent	512	0	0
	Noncoherent	512	126	154
Golay sequence	Coherent	256	56	72
	Noncoherent	256	72	112

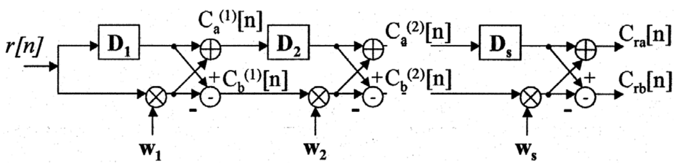

Fig. 9. Efficient Golay correlator (EGC).

This new possibility presents several advantages compared to traditional correlation algorithms and results in reduced computations. First, in traditional correlation it is necessary to perform N multiplications (N is the length of the sequence), whereas, in the EGC, only $\log_2 N$ multiplications are computed. In this way, the classical method requires $N-1$ additions, and ECG has only $2\cdot\log_2 N$. Second, the number of memory accesses in EGC is also reduced from N to $2\cdot\log_2 N$. This is an important feature, because memory access is usually the bottleneck in digital systems.

Insofar as multiplications are concerned, it is important to note that, in the developed system, correlation is performed between demodulation components and sequences with values in the set $\{-1,+1\}$, so all computations are reduced to only additions and subtractions.

IV. System Implementation

A. Low-Level Processing

The algorithm has been implemented on a Xilinx Virtex field-programmable gate array (FPGA) device [11]. The general block diagram of this implementation can be seen in Fig. 10. The system has two TI comm-port links [12] so it can communicate with an external controller module. Comm-port 0 is used for data communication between the acquisition system and the FPGA device. After analysis, it returns TOFs obtained from the two existing emissions. On the other hand, comm-port 1 operates as a command interface, allowing the external controller to modify the operation mode of the FPGA. Both ports are managed by an internal controller finite state machine and two first-in first-out memories for the purpose of transmission and reception.

The global internal controller consists of two parts, one of which executes and configures the global system, in accordance with the commands received from comm-port 1. It also sends processed information (TOFs) to the external controller. The other is a TOF measurement module based on a counter, the value of which increases with each new sample acquired. The arrival of an echo from either of the two emissions allows the count value at that moment to be stored, thus determining the TOF for the detected echo. The block diagram of this module can be seen in Fig. 11.

Demodulation is mathematically described in (4). Only component $Q_i[n]$ has been computed. Component $I_i[n]$ can be obtained from the previous one by using a two-sample delay. In this way, the demodulation process is reduced to only one correlation. The modulation symbol used, shown in (6), includes two periods of the carrier signal, with a total of 16 samples (a 50-kHz modulation carrier with a 400-kHz acquisition frequency implying 8 samples per period of the emitted signal $-M=8-$). Considering this, the implemented equation in differences (7) that describes demodulation processing can be developed. It can be seen that only the last 14 executed samples are needed. Fig. 12 shows the implementation stage, using shift registers.

$$\begin{aligned} S_Q[n] &= \left\lfloor S_{Q_{-(N-1)}}, S_{Q_{-(N-2)}}, \ldots, S_{Q_{-1}}, S_{Q_0} \right\rfloor \\ &= [1,1,0,0,-1,-1,0,0,1,1,0,0, \\ &\quad -1,-1,0,0]. \end{aligned} \tag{6}$$

$$\begin{aligned} Q_i[n] &= -\sum_{k=-2}^{-3} r[k+n] + \sum_{k=-6}^{-7} r[k+n] \\ &\quad - \sum_{k=-10}^{-11} r[k+n] + \sum_{k=-14}^{-15} r[k+n] \\ Q_i[n-1] &= -\sum_{k=-3}^{-4} r[k+n] + \sum_{k=-7}^{-8} r[k+n] \\ &\quad - \sum_{k=-11}^{-12} r[k+n] + \sum_{k=-15}^{-16} r[k+n] \\ Q_i[n] &= Q_i[n-1] - r[n] + r[n-2] + r[n-4] \\ &\quad - r[n-6] - r[n-8] + r[n-10] \\ &\quad + r[n-12] - r[n-14]. \end{aligned} \tag{7}$$

The sequence-searching block synthesizes the scheme of the simplified algorithm proposed in [10], so that a basic operation unit (OP) is defined (Fig. 13), which is used with some shift registers in the global design stage.

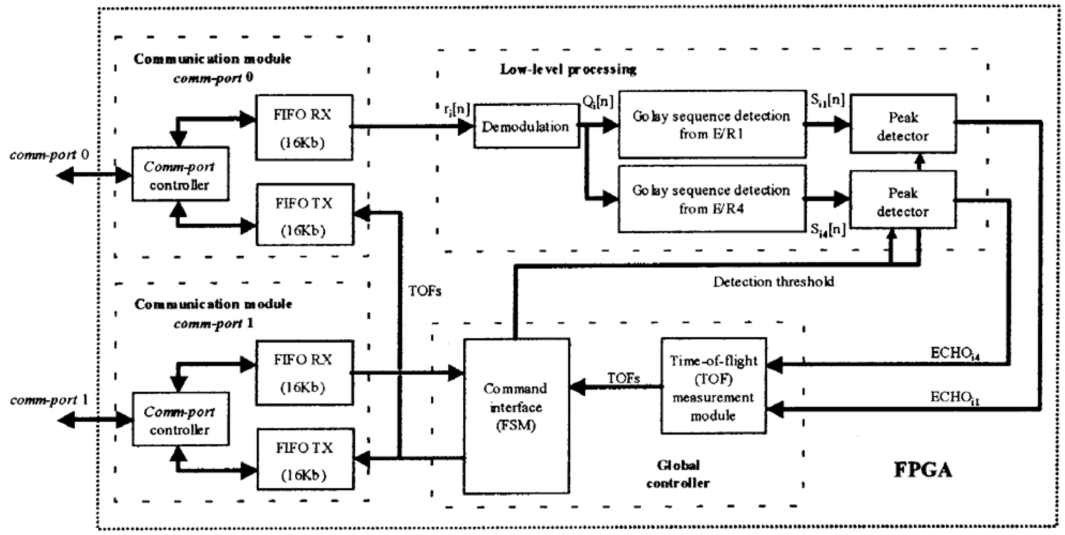

Fig. 10. General block diagram of the implemented architecture.

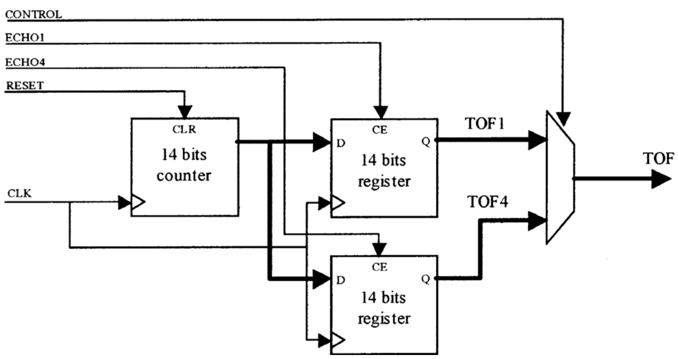

Fig. 11. Block diagram of the TOF measurement module.

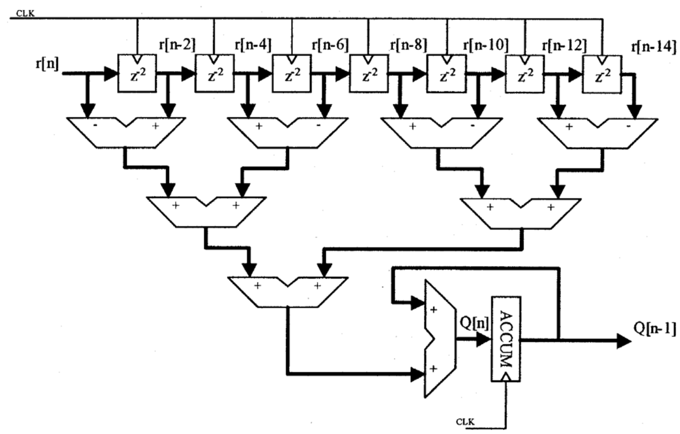

Fig. 12. Implementation of the demodulation stage.

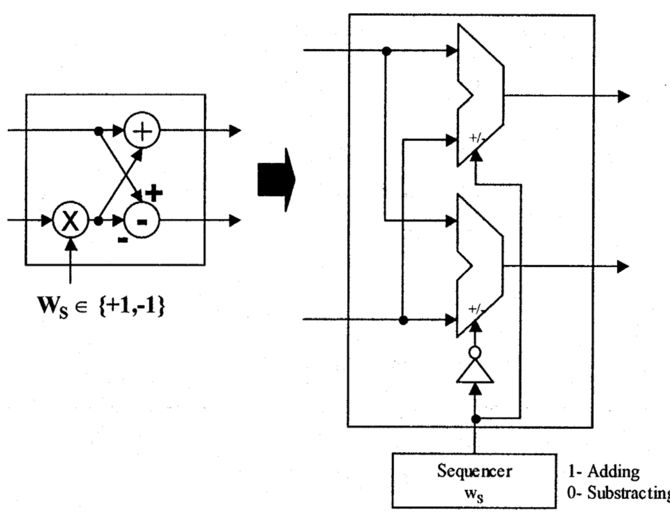

Fig. 13. Basic operation unit OP implementation.

Fig. 14 shows the general scheme of this stage. The sequence detector implementation is described for transducer i of the sensor. The system consists of two identical blocks that detect possible echoes of emissions from transducers $E/R1$ and $E/R4$ on the demodulated signal $Q_i[n]$. The described scheme is used for 32-bit Golay sequences. Nevertheless, the system can be adapted to sequences of different lengths by adding or removing OP unit stages, and instantiating delay blocks according to the progression shown.

Finally, the last stage consists of a peak detector module, the function of which is to analyze local maximums over a determined threshold. Fig. 15 shows the general module scheme. A peak is validated as an echo if its value is greater than the threshold, and if it is the maximum value in an analysis window V_0 of 16 samples. This analysis window eliminates the validation of the secondary modulation peaks as echoes. The threshold can be configured to adapt the system to certain environmental conditions, and to guarantee a correct detection of received echoes. The threshold is updated every F_o samples ($F_o = 256$ in

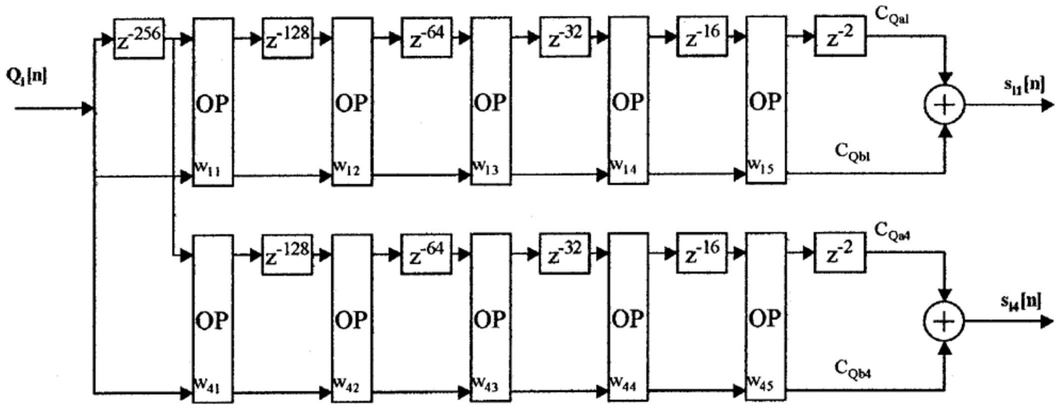

Fig. 14. Detection scheme of two Golay pairs in a transducer i.

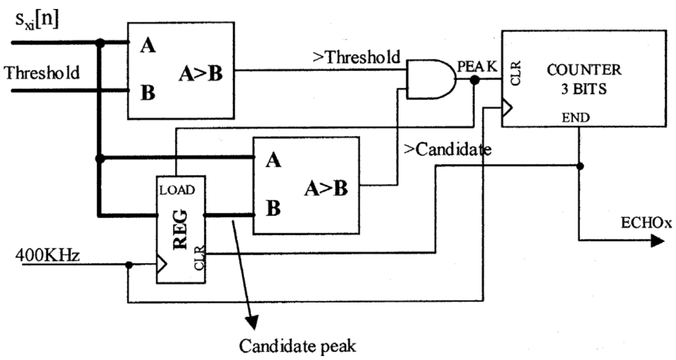

Fig. 15. Block diagram of the peak detector.

this case) in accordance with (8), so the *Threshold* value depends on the SNR in the input signal $r_i[k]$.

$$Threshold[K] = \max\left\{\frac{U_i}{FE}\cdot\Delta r_i,\, U_o\right\} \quad K = 1,\, F_o,\, 2\cdot F_o, \ldots, \tag{8}$$

where:

- *Threshold* is the final value used in the peak detector.
- U_i is the initial threshold (empirically determined at 45,000).
- FE is determined by the maximum input range ($FE = 256$).
- Δr_i is the difference between the maximum and minimum value of the signal $r_i[n]$ in the analysis window F_o.
- U_o is the minimum threshold to apply (also fixed empirically at 10,000).
- and F_o is the sample window analyzed to adapt the threshold ($F_o = 256$).

B. Pipeline Structure

In order to configure the synchronous execution of the system, a pipeline structure has been chosen as the optimum solution. The pipeline has the following four stages:

- Data search.
- Demodulation.

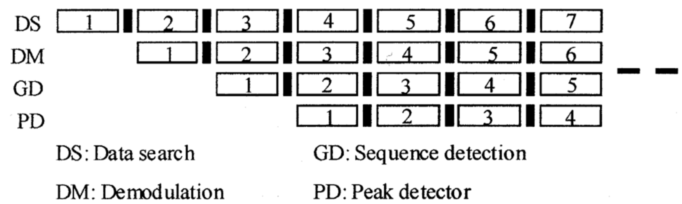

Fig. 16. Developed pipeline structure.

- Sequence detection.
- Peak detector.

Each stage takes an FPGA clock cycle for execution, thus avoiding problems of structural or data dependencies (Fig. 16).

To detect obstacles at distances of up to 5 m, 11,764 samples must be acquired at a frequency of 400 kHz. The clock frequency of the Virtex FPGA is 50 MHz and the pipeline structure provides a new sample every cycle, so processing takes 235 μs to analyze the signal in only one transducer. If processing has to be repeated for the four existing transducers in the module, the final execution time of algorithms is 940 μs.

C. Sequence Length Modification

The system designed provides the possibility of modifying the sequence length in run-time, using an external controller. This means the system can be adapted to fit the environmental circumstances. Thus, two operation modes can be defined:

- Near mode. Detected reflectors are nearer than 3 m, so 32-bit Golay complementary sequence pairs are used.
- Far mode. Detected reflectors are farther than 3 m away. Due to the increase in distance, 128-bit Golay sequences are used to improve reduced SNRs, typical in long distances.

So, the external controller configures the FPGA to adapt the operation mode, in accordance with the TOFs measured in previous emissions. The FPGA configuration is carried out using a TI comm-port link. First, a reset process is made on the FPGA, and then the new global

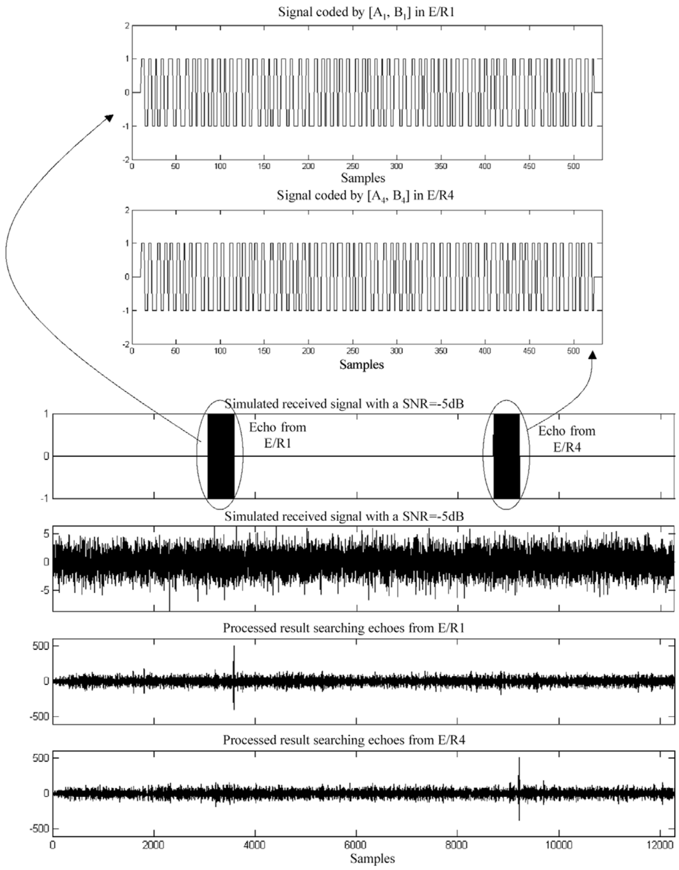

Fig. 17. Simulated detection of echoes from both emitters, $E/R1$ and $E/R4$, with a SNR = −5 dB. The sequence length used is 32 bits.

bitstream configuration is downloaded. This stage can be optimized by new partial configuration techniques on FPGAs, which allow downloading times to be reduced. Resources not used in near mode, compared to far mode, allow reflector classification and mapping algorithms to be performed [7].

V. Results

Simulations have been carried out in order to verify the suitability of algorithms proposed in this work. Fig. 17 shows a simulated reception with echoes from two 32-bit orthogonal emissions. It can be seen from the results how echoes (peaks) from both emitters ($E/R1$ and $E/R4$) can be easily identified without cross-talk interference, even in noisy environments (SNR = −5 dB in the example). The SNR supported by the system depends mainly on the sequence length used. Tests performed with 32-bit long sequences shows maximum SNR values of −12 dB.

The design has been implemented on an FPGA-based platform [13]. It is a Virtex XCV1000E device on which all the algorithms mentioned before have been developed. The results obtained with 32-bit-long sequences show that only 12% of the slices have been used, whereas this percentage increases to 32% when sequences are 128-bits long.

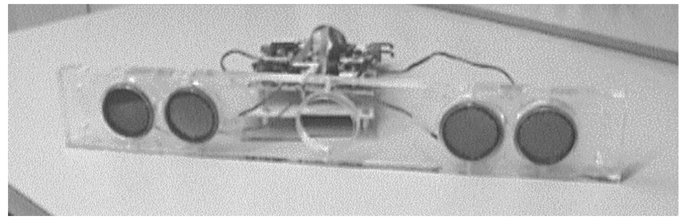

Fig. 18. General view of the sonar sensor developed.

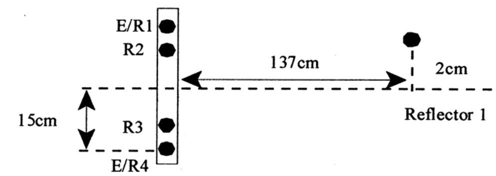

Fig. 19. Environment example with a reflector.

This implies that final designs can be optimized on lower-cost FPGA devices. Fig. 18 shows the aspect of the sonar system developed.

A real example of the system with a pole reflector is shown in Fig. 19. Initially, simultaneous emissions take place in emitters ($E/R1$ and $E/R4$), after which all the receivers ($E/R1$, $R2$, $R3$, and $E/R4$) start to process the received signal. The $E/R1$ and $E/R4$ results are shown in Figs. 20 and 21, where the following TOFs can be determined simultaneously:

- $t_{11} = 8.1125$ ms (measured in $E/R1$ for emission from $E/R1$).
- $t_{14} = 8.1375$ ms (measured in $E/R1$ for emission from $E/R4$).
- $t_{41} = 8.1375$ ms (measured in $E/R4$ for emission from $E/R1$).
- $t_{44} = 8.15$ ms (measured in $E/R4$ for emission from $E/R4$).

These TOFs have different values depending on the geometry of the proposed environment. Although echoes from both emissions overlap in the received signal, different TOFs are measured for each of them, as orthogonal Golay complementary pairs prevent cross-talk interference. Similar processing is performed in transducers R2 and R3, although it is not shown in the figures. It can be seen that real echoes are different from those obtained in simulated signals (see Fig. 5 and Fig. 17). This is due to channel and transducer effects, which have not been taken into consideration.

A statistical study has been carried out, placing an edge reflector (with a diameter of $\phi = 3.5$ cm) at a distance d on the axial axis of a transducer i. Five hundred measurements have been performed for each of the distances d; it is possible to analyze them, calculating the average value of the results obtained, as well as the standard deviation σ_i. These parameters are shown in Table II, using Golay sequences with a length of $N = 32$ bits, whereas

TABLE II
Performance in TOF Determination Using 32-bit Golay Complementary Sequences.

$N = 32$ bits	$d = 60$ cm	$d = 100$ cm	$d = 200$ cm	$d = 300$ cm
Average value (cm)	60.65 cm	100.10 cm	200.18 cm	300.53 cm
σ_i (mm)	0.0946 mm	0.1163 mm	0.6923 mm	1.0016 mm
Correct meas. (%)	100%	98%	97%	100%

TABLE III
Performance in TOF Determination Using 128-bit Golay Complementary Sequences.

$N = 128$ bits	$d = 60$ cm	$d = 100$ cm	$d = 200$ cm	$d = 300$ cm
Average value (cm)	60.05 cm	100.00 cm	200.25 cm	299.97 cm
σ_i (mm)	0.0432 mm	0.1036 mm	0.1079 mm	0.4670 mm
Correct meas. (%)	100%	99%	100%	98%

$N = 128$ bits	$d = 400$ cm	$d = 500$ cm	$D = 600$ cm
Average value (cm)	400.39 cm	500.18 cm	600.74 cm
σ_i (mm)	0.8540 mm	0.9563 mm	1.5120 mm
Correct meas. (%)	96%	97%	96%

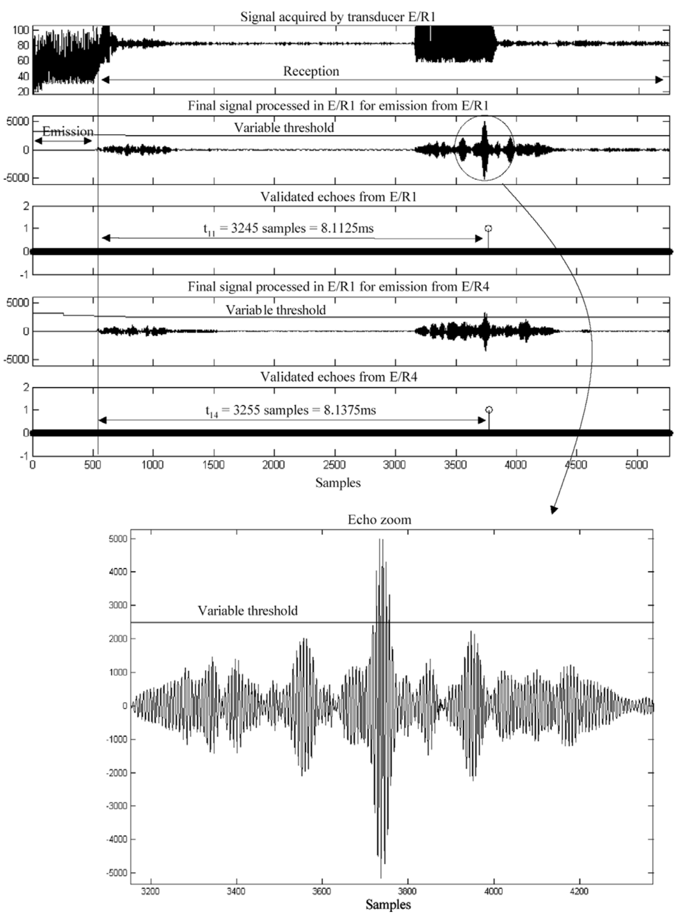

Fig. 20. Processed signal and results in transducer $E/R1$, carrying out simultaneous emission in $E/R1$ and $E/R4$.

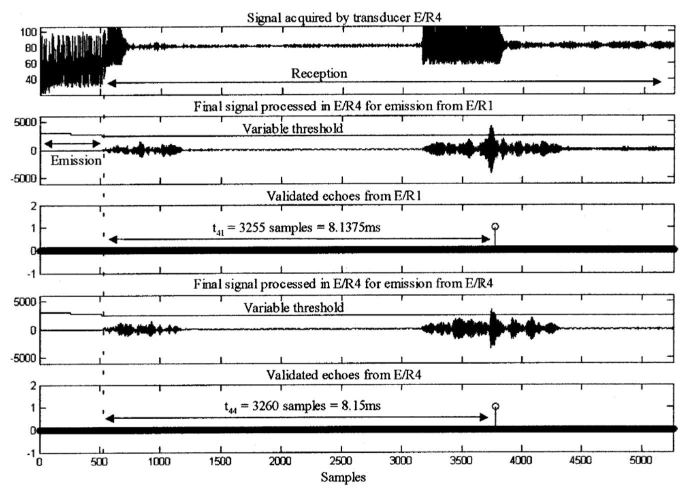

Fig. 21. Processed signal and results in transducer $E/R4$, carrying out simultaneous emission in $E/R1$ and $E/R4$.

in Table III the same data have been compiled for 128-bit Golay sequences.

Carrying out a comparison with other systems, the standard deviations σ_i obtained here are lower than those from most other works in the area [4]–[6], [14], [15]. Only more recent works [16] have achieved values of σ_i even better (around 0.2 mm at distances of 300 cm), although with a considerable increase of the computational load as they are based on reception pattern searches. This implies that reflectors must be known *a priori*, or at least be similar to the available patterns. On the other hand, the system described here does not require any initial information about reflectors. It is also important to mention that the proposed system could be improved notably by increasing the acquisition frequency f_s, which would provide greater precision without a considerable increase of the computational requirements. It should also be noted that the reflector used in these measurements is a cylinder of reduced dimensions with a specular surface; results would have been better if planes, or another type of obstacle, had been used.

Finally, as explained in Section IV about the peak detector module, there is a parameter V_o that determines the width of the analysis window used in the search for these maximum values. This parameter V_0 is equal to $2 \cdot M = 16$ samples (depending on the length of the modulation symbol), so that sidelobes from noncoherent demodulation will not be considered as echoes. Therefore, the minimum distance to be discriminated between two independent reflectors is 17 samples or, alternatively, 14.45 mm at a 400-kHz acquisition frequency f_s.

VI. Conclusions

The feasibility of multimode techniques in ultrasonic sensorial systems using Golay complementary sequences has been demonstrated. The proposed system allows simultaneous emissions in two transducers to be made, avoiding cross-talk problems. It also permits simultaneous reception in all transducers, thus being able to discriminate the emitter of the echo.

The system has been implemented on a Xilinx Virtex FPGA device. The flexibility offered by this device allows the Golay sequence length to be modified (32 or 128 bits) so that it can be adapted to the distance of the reflector in the environment. In this way, the system is optimized for any situation in run-time. Furthermore, the TOFs obtained can be used to implement high-level algorithms (reflector classification, mapping, etc.). Future work will also focus on the reduction of the transducer and channel effect on final results.

Acknowledgment

This work has been possible thanks to the Spanish Ministerio de Ciencia y Tecnología (PARMEI project, ref DIP2003-08715-C02-01) and to the Comunidad de Madrid (ENIGMA project, ref. 07T/0051/2003 1).

References

[1] K. Audenaert, H. Peremans, Y. Kawahara, and J. Van Campenhout, "Accurate ranging of multiple objects using ultrasonic sensor," in *Proc. IEEE Int. Conf. Robot. Automat.*, Nice, 1992, pp. 1733–1738.

[2] H. Hamadene and H. Colle, "Optimal estimation of the range for mobile robots using ultrasonic sensors," in *Proc. 3rd IFAC Symp. Intell. Comp. Instrum. Contr. Appl. (SICICA'97)*, Annecy, France, 1997, pp. 141–146.

[3] J. Borenstein and Y. Koren, "Error eliminating rapid ultrasonic firing for mobile robots obstacle avoidance," *IEEE Trans. Robot. Automat.*, vol. 11, no. 1, pp. 132–138, Feb. 1995.

[4] H. Peremans, A. Koenraad, and J. Van Compenhout, "A high-resolution sensor based on tri-aural perception," *IEEE Trans. Robot. Automat.*, vol. 9, no. 1, pp. 36–48, Feb. 1993.

[5] J. Ureña, M. Mazo, J. J. García, A. Hernández, and E. Bueno, "Correlation detector based on a FPGA for ultrasonic sensors," *Microprocess. Microsyst.*, vol. 23, pp. 25–33, 1999.

[6] L. Kleeman and R. Kuc, "Mobile robot sonar for target localization and classification," *Int. J. Robot. Res.*, vol. 14, no. 4, pp. 295–318, 1995.

[7] J. Ureña, M. Mazo, J. J. García, A. Hernández, and E. Bueno, "Classification of reflectors with an ultrasonic sensor for mobile robot applications," *Robot. Auton. Syst.*, vol. 29, pp. 269–279, 1999.

[8] V. Díaz, J. Ureña, M. Mazo, J. J. García, E. Bueno, and A. Hernández, "Using complementary sequences for multi-mode ultrasonic operation," in *Proc. 7th IEEE Int. Conf. Emerg. Technol. Factory Automat. (ETFA'99)*, Barcelona, 1999, pp. 599–604.

[9] B. B. Lee and E. S. Furgason, "High speed digital Golay code flaw detection system," *Ultrasonics*, vol. 21, no. 4, pp. 153–161, 1983.

[10] B. M. Popovic, "Efficient Golay correlator," *Electron. Lett. 19th*, vol. 35, no. 17, 1999.

[11] *Virtex-E 1.8V Field Programmable Gate Arrays*, Product specification, Xilinx, Inc 2000.

[12] *TMS320C4x. General-Purpose Applications. User's Guide*, Digital signal processing solutions, Application Notes, Texas Instruments Inc., 1999.

Sundance Multiprocessor Technology Ltd..

[14] A. M. Sabatini, "Active hearing for external imaging based on an ultrasonic transducer array," in *Proc. IEEE Int. Conf. Intell. Robots Syst. (IROS'92)*, Raleigh, NC, 1992, pp. 829–836.

[15] C. Papageorgiou, C. Kosmatopoulos, and T. Laopoulos, "Accurate time-of-flight measurement of ultrasonic signals for displacement monitoring applications," in *Proc. IEEE Instrum. Meas. Technol. Conf.*, St. Paul, MN, 1998, pp. 154–159.

[16] L. Kleeman, "Advanced sonar sensing," in *Proc. 10th Int. Symp. Robot. Res. (ISRR'01)*, Lorne, Australia, 2001, pp. 286–295.

Álvaro Hernández obtained his electronic engineering degree from the University of Alcalá (Spain) in 1998. In 2003, he obtained his Ph.D. degree from the University of Alcalá (Spain) and from the Blaise Pascal University (France). He is currently an Associate Professor of Digital Systems in the Electronics Department at the University of Alcalá. His research areas are multisensor integration, electronic systems for mobile robots, digital systems, and computing architectures.

Jesús Ureña received the electronics engineering (B.S.) and telecommunications engineering (M.S.) degrees from the Polytechnical University of Madrid (Spain) in 1986 and 1992, respectively, and his Ph.D. degree in telecommunications from the University of Alcalá (Spain) in 1998.

Since 1986 he has been a lecturer in the Electronics Department at the University of Alcalá. He has collaborated in several educational and research projects in the area of electronic control and sensorial systems for mobile robots and wheelchairs and in the area of electronic systems for railways. His current research areas are low-level ultrasonic signal processing, local positioning systems (LPS), and sensory systems for railway safety.

Juan Jesús García obtained his technical telecommunication engineering degree from the University of Alcalá (Spain) in 1992, and his telecommunication engineering degree in 1998 from the University of Valencia (Spain).

He has been a lecturer of analog and digital electronics in the Electronics Department of the University of Alcalá since 1994. He has worked on several public and private projects related to digital control and sensors systems, and his current areas of interest are mobile robots and multisensor integration.

Manuel Mazo received his Ph.D. degree in telecommunications in 1988, and his engineering degree (M.Sc.) in telecommunications in 1982, all of them from the Polytechnic University of Madrid (Spain).

Currently, he is a professor in the Department of Electronics at the University of Alcalá. His research areas are multisensor (ultrasonic, infrared, and artificial vision) integration and electronic control systems applied to mobile robots and wheelchairs for physically disabled people. He is an IEEE member.

Daniel Hernanz obtained his telecommunication engineering and electronic engineering degrees from the University of Alcalá (Spain) in 1997 and 2001, respectively.

He is currently an R&D engineer for GCMcom Tech. His research areas are digital signal processing and communication systems.

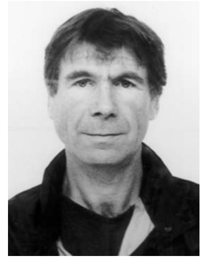

Jean-Pierre Dérutin has been a Professor at the Blaise Pascal University in Clermont-Ferrand (France) from 1994. He received his HDR degree in 1993 at the same university. He is co-director of the GRAVIR group at LASMEA- UMR 6602 CNRS- and responsible for the "Architectures et programming des machines de perception" Group. His research areas are MIMD-DM models for vision machines, their programming, and prototype methodologies for applications on these architectures. Also, he works with configurable architectures, using FPGA or SOPC devices.

Jocelyn Sérot graduated from IRESTE, Nantes, in 1989 and received the Ph.D. degree from the University of Paris-Sud in 1993. He is now Associate Professor at the Blaise Pascal University, Clermont-Ferrand, France. He works in the Computer Vision group of LASMEA (Laboratoire des Sciences et Materiaux pour l'Electronique, et d'Automatique) CNRS laboratory.